Available online at www.sciencedirect.com

ScienceDirect

Ceramics International 40 (2014) 581–590

CERAMICS INTERNATIONAL

www.elsevier.com/locate/ceramint

Effects of zircon on porous structure and alkali durability of borosilicate glasses

M. Hasanuzzaman[a,b,*], A. Rafferty[c], A.G. Olabi[a,d]

[a]Dublin City University, Mechanical and Manufacturing Engineering, Dublin 9, Ireland
[b]Bangladesh University of Engineering and Technology, Glass and Ceramics Engineering, Dhaka 1000, Bangladesh
[c]Trinity College Dublin, Centre for Research on Adaptive Nanostructures and Nanodevices, Dublin 2, Ireland
[d]University of the West of Scotland, School of Engineering, Paisley, UK

Received 3 March 2013; received in revised form 7 June 2013; accepted 10 June 2013
Available online 18 June 2013

Abstract

Additions of zircon ($ZrSiO_4$) were made to yield alkaline durable porous glasses based on the sodium borosilicate glass system. The glasses were characterised using differential thermal analysis (DTA) to identify the glass transition temperature and crystallisation temperature. The selected heat-treatment caused the glasses to phase separate by a spinodal decomposition mechanism. X-ray diffraction (XRD) was used to identify the crystalline phases. Acid leaching was used to remove the borate phase and create a porous structure. Scanning electron microscopy (SEM) revealed classic interconnected porous morphologies, while energy dispersive X-ray (EDX) analysis confirmed the presence of zirconium (Zr) in the porous silica-rich skeleton. Some of the porous glasses exhibited sharp and uniform pore distributions. Mean pore size ranged from 40 nm to 200 nm with a surface area from 5 to 35 m^2/g depending on glass composition and heat-treatment time. Zircon containing porous glasses are 3–4 times more alkali resistant than the parent sodium borosilicate glass.

Keywords: Thermal properties; Porous glass; Borosilicate glass; Phase separation; Alkali resistance

1. Introduction

Porous sodium borosilicate glass poses some unique properties, such as interconnected pore structure, chemical inertness, high mechanical and thermal stability, and high surface area, making it suitable for diversified use in the biological, electrical and pharmaceutical industries. It is known for its superior usability in membrane technology, size exclusion and affinity protein chromatography (separation science) [1–3]. For more than 30 yr, borosilicate glass has been used for the entrapment/immobilisation of high level waste from nuclear power plants and arms industries [4,5]. A low dielectric constant and negligible thermal expansion coefficient make it suitable for microelectronic packaging [6,7]. Moreover, the usage of borosilicate glass as a reinforced matrix component in composites to improve mechanical properties is widely accepted [8]. Increasing the chemical durability is one of the major challenges for porous borosilicate glass, to make it suitable and re-usable for many other applications. Borosilicate glass is known for its phase separation characteristics, thus enabling pore sizes of micro- meso- and macro-pore size, depending on the heating cycle [9].

The sodium borosilicate glass system is known to undergo amorphous phase separation (APS) by the spinodal decomposition mechanism [10]. Porous glass is derived from glass that is heat-treated to form two interconnecting phases: a silica-rich phase, and an alkali-rich borate phase. The heat-treated glass is then leached selectively to remove one of the phases. The heat-treatment step and leaching conditions can be adjusted to achieve the desired pore size, pore volume, and surface area. Therefore, porous glass based on the sodium borosilicate system can be tailor-made to required specifications with specific pore sizes over a wide range, thus offering flexibility in terms of end applications.

*Corresponding author at: Dublin City University, Mechanical and Manufacturing Engineering Dublin 9, Ireland. Tel.: +353 1 7007718; fax: +353 1 7007148.
E-mail addresses: hasanum2@mail.dcu.ie, hasanum2@gmail.com (M. Hasanuzzaman).

0272-8842/$ - see front matter © 2013 Elsevier Ltd and Techna Group S.r.l. All rights reserved.
http://dx.doi.org/10.1016/j.ceramint.2013.06.039

As was stated earlier, porous silica glass with improved alkali-resistance has been the subject of many investigations. Up to 1 N NaOH is desirable for cleaning and sanitisation of chromatography columns used in the biopharmaceutical industry [11]. However, silica is attacked by alkali. This results in pore enlargement, leading to inaccurate separations and eventually to degradation of the silica support. Stout used a chemical precursor (containing zirconia) to impregnate the pores and coat the surface of glass to improve its durability [12]. There are a number of different types of precursor available, in the form of a solution containing ZrO_2 and organics. After coating, the organics are removed by heating to leave a layer of ZrO_2 bonded to the silica surface. This is a convenient method, since porous glass can be easily dipped in solution. Dipping under vacuum enables impregnation of pores, thereby providing a surface mosaic of zirconia and silicon oxide, which according to Jungbauer [11] can withstand short term use at pH 9.0. Murakami has also pursued a surface alteration approach [13], whereby porous glass is formed (by a traditional glass-making route) and then immersed in a solution of zirconium alcoholate to form a thin film of the zirconium salt, followed by hydrolysing, drying, calcining and formation of ZrO_2 polymer on the surface of the porous glass. Coating with zirconia in this way results in a slight decrease in pore diameter/pore volume, as the inner pore walls are coated. The alkali resistance is quoted as reduced percentage of sample when treated with zirconium tetra (n-butoxide) (1% aq. at 50 °C for 1 h), and for the material, this value was 7.3%, compared to 28.4% over the non-treated glass. Eguchi et al. continued the trend of using zirconia to improve the alkali durability of silica-based glass systems [14]. Rather than coating the glass surface however, the approach involved adding zirconia powder to the starting material composition. Wada et al. also made additions of zirconia to silicate glass, using sol–gel glasses [15]. McNeff et al. used spray drying as a technique to spray dry colloidal zirconia and generate zirconia microspheres [16]. The microspheres were modified with ethylenediamine-N,N-tetra (methylenephosphonic acid) (EDTPA) to create a cation-exchange chromatographic support. Porous metal oxides of 15–100 μm in average diameter with pore sizes ranging from 40 to 60 nm and surface areas from 10 to 50 m^2/g were prepared for the preparative purification of biomolecules.

Previously, these authors have attempted to increase the zirconia content in the porous glass by modifying the initial composition using a higher amount of alkali oxide (10 wt% of Na_2O) [17]. Although zirconia was found in the porous glass, the phase separation occurred by a nucleation and growth process and yielded low pore connectivity. Zircon ($ZrSiO_4$) could be a possible candidate to replace zirconia as it is more likely to affinitise with silica and remaining part of the glass skeleton formed during leaching. In this study, the thermal behaviour of sodium borosilicate glasses with addition of zircon was investigated, which to the best of our knowledge, has not been previously reported. A comparison was also made with zirconia-containing glass of similar composition. Heat-treatment times and temperatures were optimised to achieve well-defined porous morphologies.

2. Experimental

2.1. Glass preparation

The compositions of glasses prepared in this study are detailed in Table 1. Compositions AA–EE involve substitution of SiO_2 with gradually increasing amounts of $ZrSiO_4$, keeping the content of Na_2O at 6 wt% and B_2O_3 at 25 wt%. Composition E-II was the same as EE, but with ZrO_2 replacing $ZrSiO_4$. SiO_2, B_2O_3, Na_2CO_3, ZrO_2 and $ZrSiO_4$ powders were procured from Sigma-Aldrich (Ireland). The glass reagents were ball-milled for 14 h. The mixed batches were melted in zirconia crucibles (Almath Ltd., UK) at 1450 °C for 2 h in an electric furnace. The melts were then water-quenched to produce frit. The glass frits were crushed in a ball mill for 12 h. The resultant powder was sieved to a particle size > 45 μm < 212 μm.

2.2. Thermal analysis

Differential thermal analysis (DTA) (Stanton Redcroft, UK) was used to measure the glass transition temperature (T_g) and to investigate the crystallisation behaviour. Heating rates of 10, 15, and 20 °C/min were employed using 30 mg of sample and alumina as a reference.

2.3. X-ray diffraction analysis (XRD)

Non heat-treated and heat-treated glass powders were analysed using XRD. A Bruker advanced D8 X-ray diffractometer with Ni-filtered Cu Kα radiation of wavelength 1.5406 Å at 40 kV and 40 mA was used to measure the XRD patterns with a step size of 0.1° in a range of 2θ values from 10 to 80° at scanning speed of 10 s/step. Crystalline phases present in heat-treated glass samples were identified by the positions listed in the joint commission on powder diffraction standards (JCPDS) files.

2.4. Heat treatment

Thermal treatment to induce phase separation was carried out on glass powder using a horizontal tube furnace (Carbolite Ltd., Sheffield, UK) at a heating rate of 10 °C/min. The dwell

Table 1
Composition of glasses in wt%.

Glass	SiO_2	B_2O_3	Na_2O	ZrO_2	$ZrSiO_4$
AA	69	25	6	0	0
CC	62	25	6	0	7
DD	58	25	6	0	11
EE	54	25	6	0	15
E-II	54	25	6	15	0

temperature was fixed at 650 °C. The dwell times used ranged from 14 h to 63 h.

2.5. Glass leaching

A heating bath, magnetic stirrer, and condenser were used to conduct glass leaching experiments. The heat-treated glasses were first immersed in 1 N HNO_3 for 24 h at 95–98 °C to remove the borate phase, then in 3 N H_2SO_4 for 24 h at 95–98 °C to dissolve colloidal zirconia, and finally the gelated SiO_2 was washed out with 0.5 N NaOH for 5 h at 25 °C. An H_2SO_4 leaching step was found to be unnecessary for $ZrSiO_4/ZrO_2$ free compositions. A magnetic stirrer was used to prevent the glass powder from settling on the bottom of the flask and to make leaching more effective. Following leaching, the resultant glass powders were washed with water several times and dried for 12 h at 120 °C.

2.6. Pore characterisation using mercury porosimetry

The experiments were performed on leached glass using mercury porosimetry (Autoscan-33 Porosimeter, Quantachrome, UK). Mercury intrusion and extrusion over a range of pressures (0–33000 PSIA) was performed, to determine pore sizes, pore volumes, pore surface areas, and pore distributions.

2.7. Pore characterisation by BET nitrogen adsorption analysis

Surface area, porosity, and average pore size of the selected leached glass samples were measured using a Nova 4200e surface area and pore size analyser (Quantachrome Instruments, UK). The porous glass samples were prepared by drying under vacuum at 200 °C for 2 h to remove adsorbed contaminants (especially water and carbon dioxide) which were acquired from atmospheric exposure.

2.8. Scanning electron microscopy (SEM) and energy dispersive X-ray spectroscopy (EDXS)

Pore morphologies and pore sizes of the leached glasses were observed using SEM (EVO LS15, Carl Zeiss NTS GmbH, Germany).

An Oxford instruments (Oxford INCA Energy 350) microanalysis suite EDXS was used to detect the elements present in porous glasses. Rectangular acquisition with 180 s live time in 0–10 KeV of spectrum range was used for the quantitative measurement. An acceleration voltage of 10 keV and beam current of around 100 pA was used for analysing all specimens.

2.9. Alkali resistance testing

The alkali resistance of porous glass samples was measured by incubating a 1 ml volume of sample in 10 ml of an aqueous sodium hydroxide solution (0.5 N) for 24 h. Following this, the leachant was neutralised with 1 N HCl acid and then washed in deionised water and dried at 100 °C for 18 h. After drying, each sample was weighed to an accuracy of 0.1 mg. The weight loss was then calculated in milligrams per square decimetre (mg/dm^2) using the surface area data from porosimetry.

3. Results and discussion

3.1. Thermal analysis

Heating rates of 10, 15, and 20 °C/min were employed for all glass compositions to investigate the difference in thermal behaviour while keeping the sample size 30 mg (constant). Some authors have found that T_g depends on heating rate, and shifts towards a higher temperature with increased heating rate [18]. Dodd [19] argued that increasing heating rate decreases the resolution between the adjacent peaks, hence slower heating rates are preferable.

(i) Glass AA ($69SiO_2$–$25B_2O_3$–$6Na_2O$)

Fig. 1 shows the DTA curve of glass AA at heating rates of 10, 15, and 20 °C/min. For a heating rate of 10 °C/min, a change in slope was observed from about 478 °C to 520 °C. This change in slope is attributed to the glass transition temperature. A broad exothermic event is observed in the range 740–900 °C, believed due to surface crystallisation. The exothermic peak did not become appreciably sharper for DTA analysis of finer particle size (< 45 μm), indicating a weak surface crystallisation mechanism.

(ii) Glass CC ($62SiO_2$–$25B_2O_3$–$6Na_2O$–$7ZrSiO_4$)

Onset of a broad exothermic event was detected at around 640 °C for a heating rate of 10 °C/min, followed by subsequent successive slope changes as shown in Fig. 2. This exothermic broadening is not prominent for heating rates of 15 and 20 °C/min. Small details may be lost with rapid heating rates [20]. The exothermic event observed at around 640 °C may be due to the formation of tetragonal zirconia.

(iii) Glass DD ($58SiO_2$–$25B_2O_3$–$6Na_2O$–$11ZrSiO_4$)

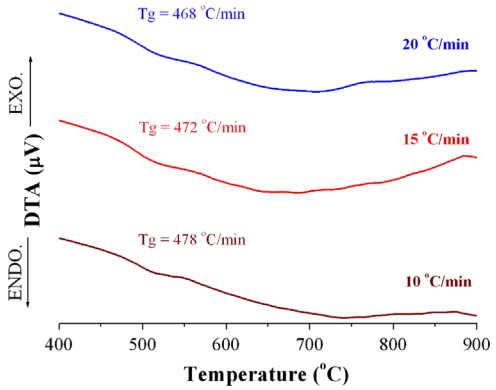

Fig. 1. DTA curve of glass AA at heating rates of 10 °C/min, 15 °C/min and 20 °C/min.

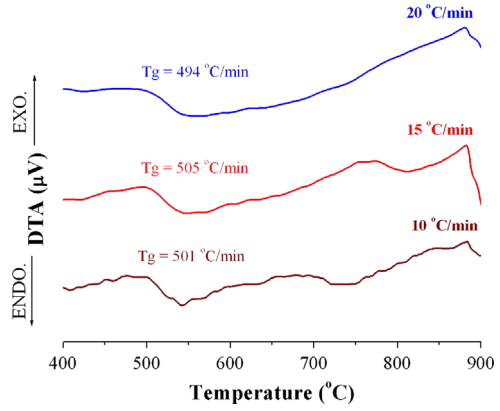

Fig. 2. DTA curve of glass CC at heating rates of 10 °C/min, 15 °C/min and 20 °C/min.

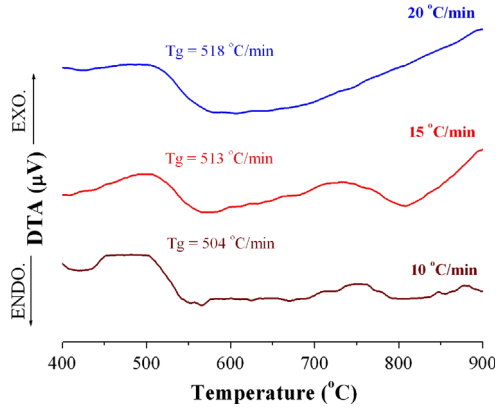

Fig. 3. DTA curve of glass DD at heating rates of 10 °C/min, 15 °C/min, and 20 °C/min.

A change in slope was observed at about 504 °C (T_g) and continues until it plateaus out at around 550 °C (heating rate 10 °C/min) (see Fig. 3). The change in slope associated with T_g became more pronounced for higher heating rates. A broad exothermic peak was observed in the range 680–800 °C. This exothermic event is believed due to the formation of tetragonal zirconia. When the heating rate was increased, this exothermic event became less noticeable. This onset of a second exothermic event at about 840 °C is attributed to the precipitation of cristobalite. The broad nature of the exothermic events is indicative of surface crystallisation.

(iv) Glass EE ($54SiO_2$–$25B_2O_3$–$6Na_2O$–$15ZrSiO_4$)

Fig. 4 shows the DTA analysis of glass EE. The changes in the curve became more conspicuous for increased heating rates. For the heating rate of 15 °C/min, a change in slope was observed at about 497 °C (T_g) and continued until it plateaus at approximately 600 °C. A sharp exothermic peak observed at 667 °C is attributed to crystallisation. The sharp nature of this peak, denoted as maximum crystallisation temperature (T_p), is indicative of bulk crystallisation [21–23]. This sharp peak was not observed for glass AA which contained no $ZrSiO_4$, so clearly the zircon

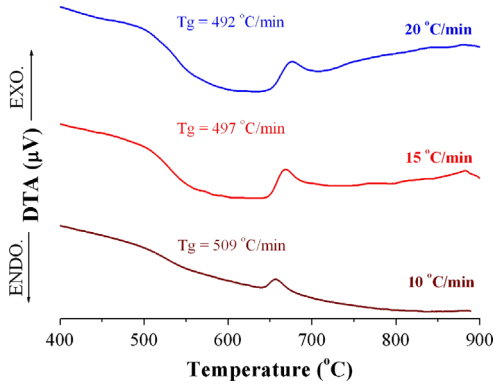

Fig. 4. DTA curves of glass EE at heating rates of 10 °C/min, 15 °C/min and 20 °C/min.

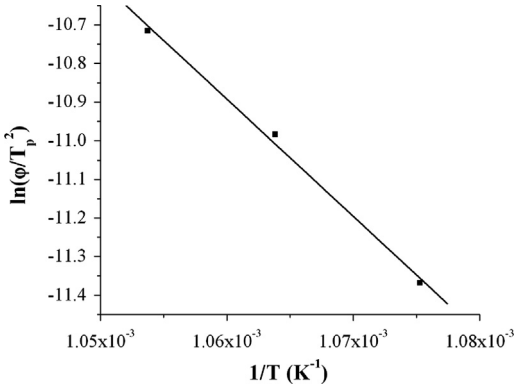

Fig. 5. Determination of E_c/R for glass EE using the Kissinger method.

is promoting bulk crystallisation. It is also evident that T_g increased incrementally with increasing $ZrSiO_4$ content from 478 °C to 509 °C. It is known that additions of ZrO_2 increase the number of bridging oxygen per silicon atom. The presence of Zr^{4+} ions impart a higher packing density and push up T_g [24].

When sharp crystallisation peaks are present, the Avrami number (n) can be calculated using Eq. 1 below, which is an accepted method to determine crystallisation mechanisms. A value of approximately 1 indicates surface crystallisation, whereas an n value >3 indicates bulk crystallisation [23]. In order to calculate the Avrami number, the activation energy (E_c) for crystallisation was calculated using the Kissinger equation [25] which is based on crystallisation peak temperature (T_p) and DTA heating rate (φ):

$$\ln\frac{\varphi}{T_p^2} = -\frac{E_c}{RT_p} + const. \quad (1)$$

The activation energy was obtained from the slope of $\ln(\varphi/T_p^2)$ versus $1/T_p$ as shown in Fig. 5. Table 2 presents the raw data required to plot Fig. 5. The activation energy (E_c) was calculated as 253 kJ/mol. By way of contrast, it is

Table 2
The results of DTA measurements for glass EE and the calculated Avrami number.

Heating rate, φ (°C/min)	Crystallisation peak temperature, T_p (°C)	ΔT (°C)	Avrami number (n)
10	657	15	4.74
15	667	17	4.28
20	676	19	3.90

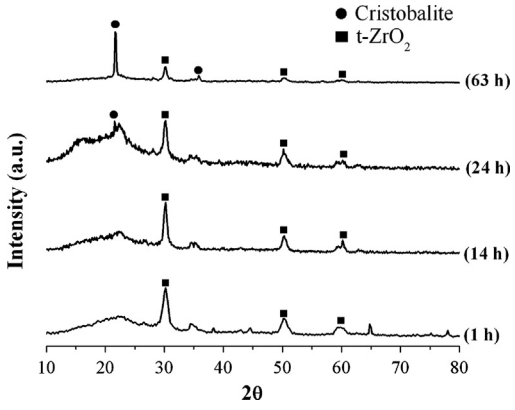

Fig. 6. XRD patterns of glass EE heat treated at 650 °C for different time periods (1 h, 14 h, 24 h and 63 h).

worth noting that Kukizaki [21] reported an E_c value of 215 kJ/mol for the $70SiO_2$–$8.5B_2O_3$–$7.3Na_2O$–3CaO–$8Al_2O_3$ glass system.

The Avrami numbers, n, calculated from Eq. 1 are listed in Table 2. The n value of glass EE is >3 for all heating rates which indicates bulk crystallisation. Kukizaki [21] obtained n values of 4.2, 3.8, and 3.7 for heating rates of 10, 15 and 20 °C/min respectively for his glass system.

XRD analysis was performed on glass composition EE to identify the crystallisation phases related to the exothermic peak observed in Fig. 4. The samples were heat treated at 650 °C, i.e. T_p onset, for various durations (1 h, 14 h, 24 h and 63 h). Peaks assigned to tetragonal ZrO_2 ($2\theta = 30°$, 51°, 60°) [JCPDS 02-0733] were identified for the sample heated at 650 °C for 1 h, 14 h, 24 h and 63 h (see Fig. 6). The peaks at $2\theta = 21.8°$, 28.5°, 36° [JCPDS 01-0438, 03-0267] are attributed to cristobalite. For heat-treatments ≤24 h, the cristobalite peaks exhibit low intensities compared with the tetragonal ZrO_2 peaks. For heat-treatment durations of 24 h $< t <$ 63 h, the intensity of the cristobalite peaks increase. Crystallisation of cristobalite predominates over crystallisation of tetragonal ZrO_2 for heat-treatment times ≥24 h. Therefore, it can be considered that the T_p observed in Fig. 6 is due to crystallisation of tetragonal zirconia.

(v) Glass E-II ($54SiO_2$–$25B_2O_3$–$6Na_2O$–$15ZrO_2$)

Fig. 7 presents the DTA analysis of the glass powder sample E-II. For a heating rate of 10 °C/min, a change in slope was observed at approximately 511 °C (T_g) and continued to 563 °C. Glass E-II and EE (6 wt% Na_2O, 15 wt% $ZrSiO_4$) showed similar T_g values, indicating that the presence of zircon or zirconia in the glass has an almost equal impact on T_g. Exothermic broadening begins at approximately 650 °C and is likely associated with surface crystallisation [22,23,26,27]. Of note is the absence of a sharp exothermic peak, as compared with glass EE (6 wt% Na_2O, 15 wt% $ZrSiO_4$) which exhibited a sharp peak at around 660 °C.

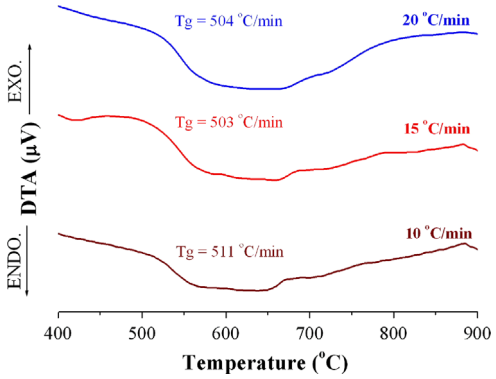

Fig. 7. DTA curve of glass E-II at heating rates of 10 °C/min, 15 °C/min and 20 °C/min.

3.2. Porosimetery

3.2.1. Pore characterisation by mercury porosimetry

(i) Glass AA ($69SiO_2$–$25B_2O_3$–$6Na_2O$)

In Fig. 8(a–e), the X-axis represents the pore diameter on a log scale. The Y-axis ($dV/d \log P$) represents the change in volume of intruded mercury with respect to the log of pressure required to force mercury into the pores. The pink line shows the mercury intrusion; a gradual uptake followed by a sharp uptake, as a large number of pores are filled at once. As can be seen from Fig. 8a, the pore-size distribution is narrow and encompasses pores of 45–95 nm. With increasing heat-treatment dwell time the mean pore-size increased (see Table 3). This is due to coarsening of the phase separated structure [1]. As the pore size increases, the surface area decreases. Small interconnected pores make a greater contribution to the surface area, compared to larger ones.

It is worth noting the circled region in Fig. 8a, which show two small peaks, and two corresponding uptakes in mercury intrusion. The volume contribution of the corresponding pores is negligible. However, this is due to there being a very large number of very small, low volume pores. In other words, the 'pore number fraction' of these small pores is very high. Pore number fraction data is generated by the porosimetry software and shows peaks for large numbers of pores, i.e. on a number basis, not volume. Oftentimes, the 'volume' and 'number fraction'

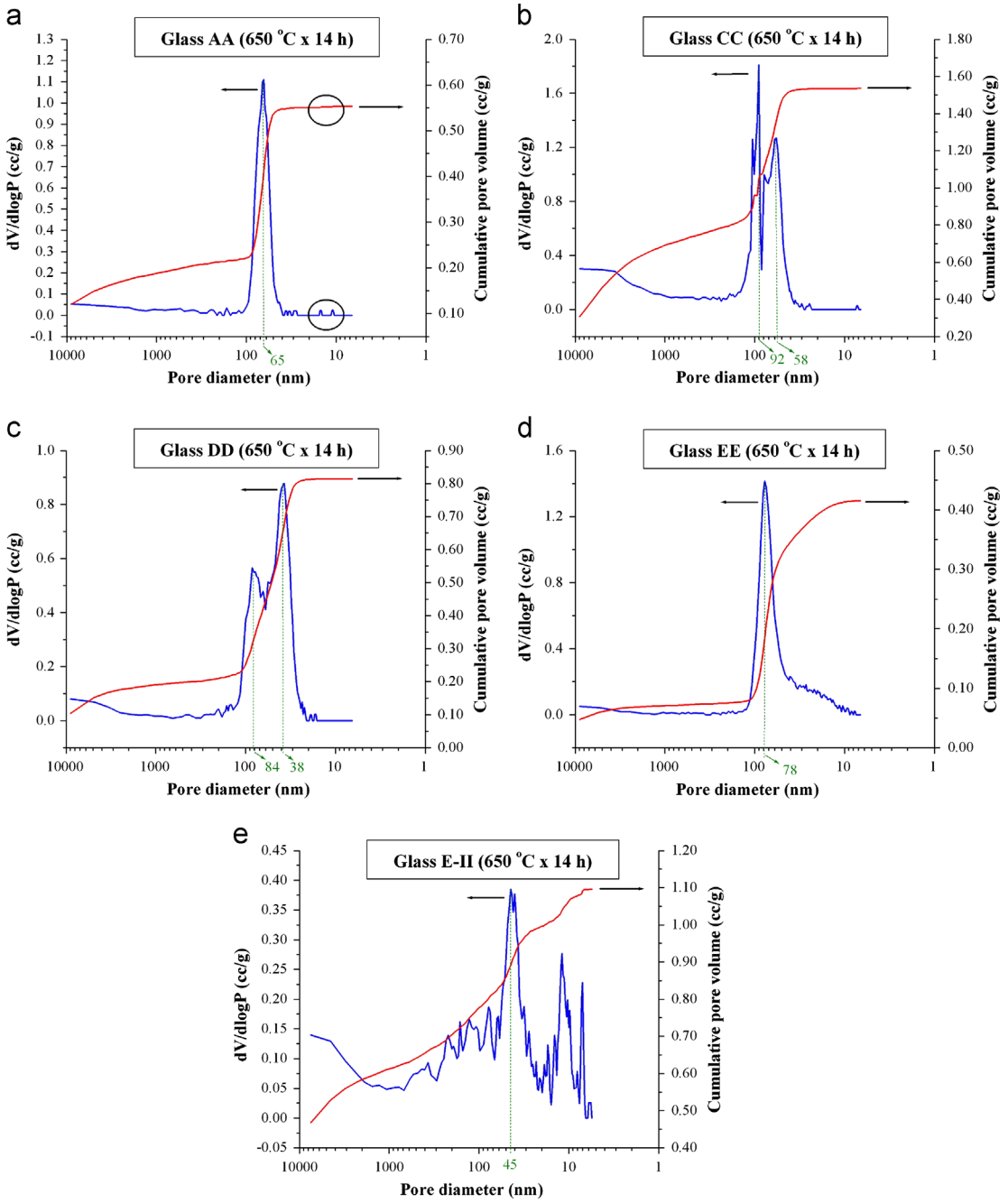

Fig. 8. Pore-size distribution curves of porous glasses: (a) AA, (b) CC, (c) DD, (d) EE and (e) E-II (heat-treated at 650 °C for 14 h) determined by mercury intrusion.

peaks overlap. In other cases, we see a separate peak for pore number fraction. This usually occurs when there is gel trapped in pores. The ideal scenario, for the purpose of this work, is to have perfect overlap between volume and number fraction peaks, i.e. a porous material containing a large number of high volume pores in the ~100 nm range.

(ii) Glass CC ($62SiO_2$–$25B_2O_3$–$6Na_2O$–$7ZrSiO_4$)

A bi-modal pore distribution is observed in the range 40–140 nm for glass CC as shown in Fig. 8b. Similar to glass AA, the mean pore-size increased for longer heat-treatment times, and the surface area decreased. The total pore volume increased initially (from 14 h to 24 h). With a further increase in heat-treatment dwell time (63 h) at 650 °C, the total pore volume then decreased significantly. This decrease in pore volume is not easily explained. It may be due to incomplete leaching or, more likely, the occurrence of surface crystallisation. The surface area of glass CC is about double that of glass AA. This is believed due to the higher pore volume and higher percentage of porosity.

(iii) Glass DD ($58SiO_2$–$25B_2O_3$–$6Na_2O$–$11ZrSiO_4$)

Glass DD exhibits a bi-modal distribution in the range 25–115 nm as shown in Fig. 8c. The pore-size distribution

Table 3
Effect of thermal treatment on pore characteristics of glass AA, CC, DD, EE and E-II measured by mercury porosimetry.

Glass	Thermal treatment		Mean pore diameter (nm)	Total surface area (m^2/g)	Pore volume (cm^3/g)
	Temperature (°C)	Period (h)			
AA	650	14	80	12	0.553
AA	650	24	115	8	0.678
AA	650	63	139	5	0.566
CC	650	14	112	25	1.537
CC	650	24	151	17	1.605
CC	650	63	173	8	0.719
DD	650	14	57	28	0.814
DD	650	24	56	22	0.580
DD	650	63	100	15	0.823
EE	650	14	52	31	0.407
EE	650	24	65	29	0.964
EE	650	63	115	13	1.024
E-II	650	14	41	35	1.096
E-II	650	24	58	18	0.678
E-II	650	63	139	8	0.896

became broader and shifted towards a larger pore size range with increasing heat-treatment dwell time. The surface area decreased with increasing heat-treatment dwell time at 650 °C. The total pore volume decreased initially (from 14 h to 24 h) and then increased again with a further extension of heat-treatment dwell time (63 h), whilst an increase in pore size was also observed (from 56 to 100 nm).

(iv) Glass EE ($54SiO_2$–$25B_2O_3$–$6Na_2O$–$15ZrSiO_4$)

A single sharp peak is centred around 78 nm for glass EE, with a narrow pore-size distribution in the range 50–100 nm (see Fig. 8d). The total pore volume increased with increasing heat-treatment dwell time, whilst the surface area decreased.

(v) Glass E-II ($54SiO_2$–$25B_2O_3$–$6Na_2O$–$15ZrO_2$)

There are multiple peaks with the main one occurring in the range 30–60 nm (see Fig. 8e). These peaks correspond to mesopores, and could be as a result of trapped gel which has not been fully removed during leaching. Silica gel is known to exhibit mesoporosity [28]. As can be seen from Table 3, the mean pore size increased and the surface area decreased with increasing heat-treatment dwell time.

For the glasses studied here, the mean pore size decreased when $ZrSiO_4$ was added ≥11 wt%. Kukizaki [21] with a similar glass system found that addition of ZrO_2 increases the activation energy for diffusion in phase separation at a given heat-treatment time. A similar effect is expected for $ZrSiO_4$ and thus, the mean pore diameter of the resultant porous glass is reduced. Fig. 9 shows the relationship between mean pore diameter and square root of heat-treatment time at 650 °C for glass series AA–EE. For each glass in the series, mean pore diameter is linearly related to square root of heat-treatment time.

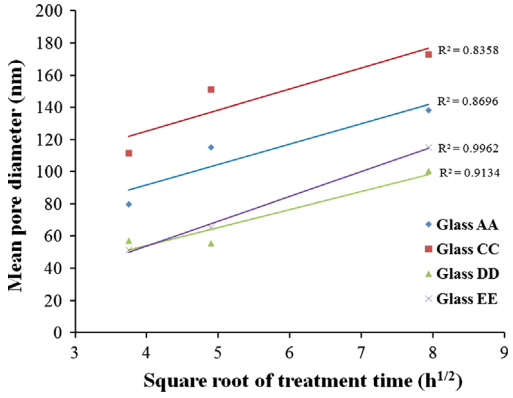

Fig. 9. Relationship between heat-treatment time and pore diameter for glass series AA–EE after heat-treatment at 650 °C.

Table 4
Effect of thermal treatment on pore characteristics of different glass compositions measured by nitrogen adsorption.

Glass	Thermal treatment		Mean pore diameter (nm)	Specific surface area (m^2/g)	Pore volume (cm^3/g)
	Temperature (°C)	Period (h)			
AA	650	14	8	28	0.058
AA	650	24	9	22	0.048
AA	650	63	10	18	0.045
EE	650	14	22	30	0.165
EE	650	24	7	168	0.310
EE	650	63	22	22	0.122
E-II	650	14	10	98	0.253
E-II	650	24	10	82	0.205
E-II	650	63	17	14	0.060

3.2.2. *Pore analysis by BET nitrogen adsorption analysis*

For analysis of macroporous material (pore diameter > 50 nm), mercury porosimetry is considered most useful and reliable [29]. A very large range of pore sizes can be analysed, nominally 6–10,000 nm. Furthermore, an intrusion cycle can typically generate in excess of 600 data points, leading to well-defined and accurate data curves. BET is best-suited to studies of micro (< 2 nm) and meso (2–50 nm) pores. According to the literature [30], pores in the range 0.35–200 nm can be measured with nitrogen adsorption. However, depending on the material, it can be challenging to generate comprehensive data for distribution of pores > 100 nm. On the other hand, BET can provide valuable information on pores resulting from trapped gel species, or secondary pores which form in the walls of the main porous skeleton (both of these pore types are often in the meso-range). Nitrogen adsorption porosimetry was conducted on selected glasses; base glass (glass AA) and glasses containing 15 wt% ZrO_2/$ZrSiO_4$ (glass E-II and glass EE), to compare against results obtained using mercury porosimetry (see Table 4). The mean pore diameters measured are an order of magnitude lower than those measured using porosimetry.

The total pore volumes measured using porosimetry were significantly higher compared to those measured by nitrogen adsorption. This is due to porosimetrys capacity to

comprehensively measure porosity in the size range of interest, i.e. 40–200 nm. The larger pores which are within the porosimeters measurement range are expected to make a greater contribution towards the total pore volume. The actual measurement range during nitrogen adsorption varied from sample to sample. A general trend was found, where the surface area values of some samples were in good agreement with those measured using porosimetry, for example, sample EE (14 h at 650 °C). For this sample, the actual gas adsorption measurement range reached ~95 nm, and for this reason the two result sets show better agreement. In some cases, however, no gas adsorption measurement data was returned for pore diameters > 40 nm, as in the case of glass EE (24 h at 650 °C), for example. When this occurred, the narrow measurement range focussed on mesoporosity, resulting in a surface area measurement of 168 m^2/g, as compared with 29 m^2/g when measured using porosimetry. This demonstrates the difficulty in making comparisons between the data sets, without careful consideration of the different parameter involved. Furthermore, it must be remembered that at the very low end, i.e. < 10 nm, the gas adsorption method can measure pores which are beyond the range of the porosimeter. Both results are valid, but there cannot be matching data because they are concentrated on different pore ranges. The surface area value generated by porosimetry is generally found to agree with gas adsorption when there are no very small pores present, i.e. < 10 nm. When these pores are present, they are outside of the porosimeters measurement range and the surface area value is therefore artificially low.

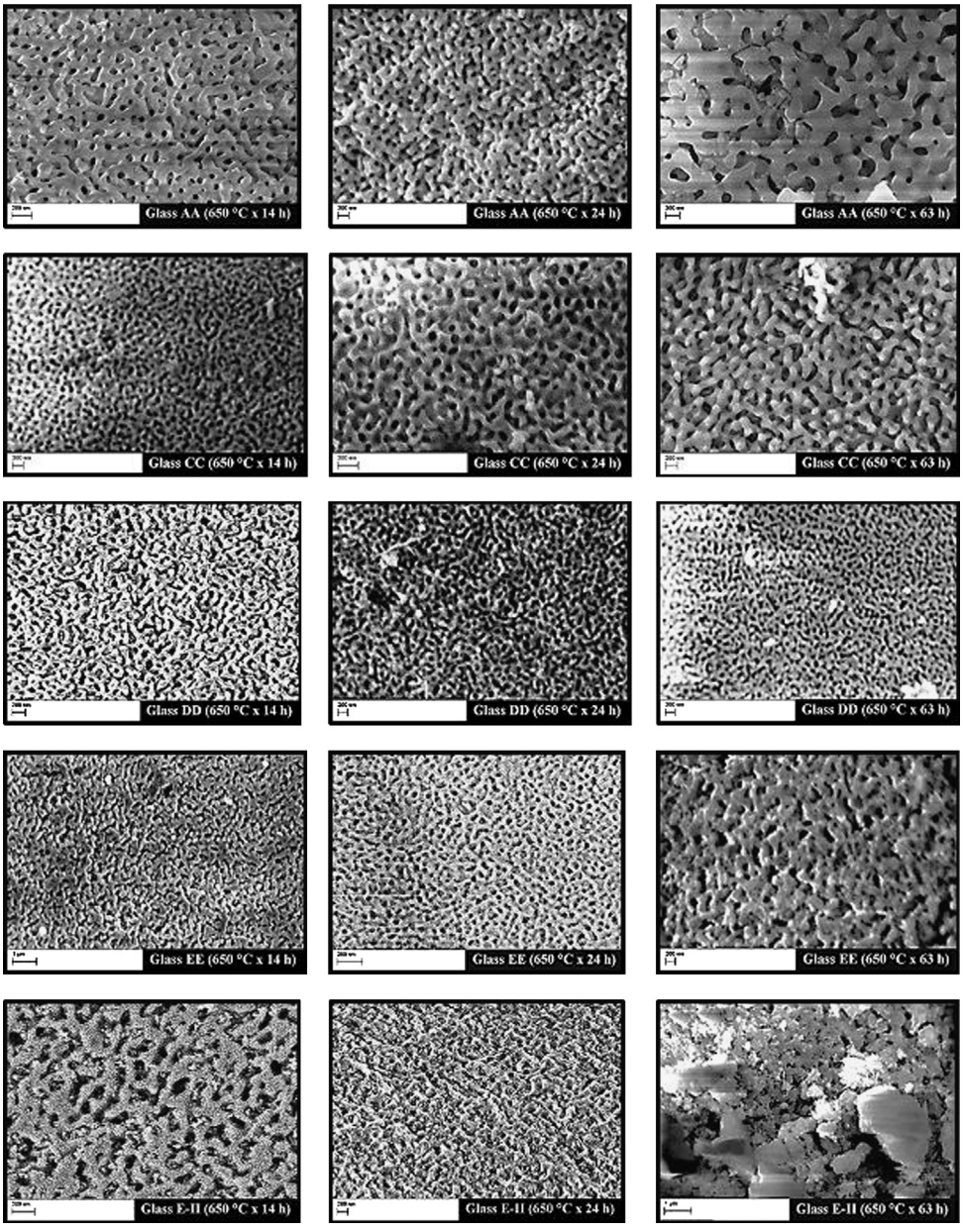

Fig. 10. SEM photographs of heat-treated glass AA, CC, DD, EE, and E-II after leaching.

Table 5
Elemental analysis of porous glasses by EDXS.

Glass	Thermal treatment		Si (wt%)	Na (wt%)	Zr (wt%)	O (wt%)
	Temperature (°C)	Period (h)				
AA	650	14	47	1	–	53
AA	650	24	45	1	–	54
AA	650	63	47	1	–	52
CC	650	14	43	2	–	55
CC	650	24	55	1	–	44
CC	650	63	43	1	–	56
DD	650	14	44	1	–	55
DD	650	24	43	–	–	57
DD	650	63	41	1	–	58
EE	650	14	32	–	22	46
EE	650	24	26	2	24	48
EE	650	63	24	1	28	47
E-II	650	14	29	1	23	48
E-II	650	24	34	–	18	49
E-II	650	63	38	–	20	42

Table 6
$ZrSiO_4/ZrO_2$ content and alkali resistance for porous glass of AA, CC, DD, EE and E-II.

Glass	Thermal treatment		$ZrSiO_4$ content (wt%)	ZrO_2 content (wt%)	Weight loss per total surface area (mg/dm^2)
	Temperature (°C)	Period (h)			
AA	650	14	0	0	0.35
AA	650	24	0	0	0.28
AA	650	63	0	0	0.24
CC	650	14	7	0	0.29
CC	650	24	7	0	0.24
CC	650	63	7	0	0.49
DD	650	14	11	0	0.30
DD	650	24	11	0	0.27
DD	650	63	11	0	0.47
EE	650	14	15	0	0.09
EE	650	24	15	0	0.18
EE	650	63	15	0	0.21
E-II	650	14	0	15	0.19
E-II	650	24	0	15	0.33
E-II	650	63	0	15	0.23

3.3. Scanning electron microscopy (SEM) and energy dispersive X-ray spectroscopy (EDXS)

Classical skeleton-like microstructures with highly connected pores are observed for porous glasses of glass series AA–EE (see Fig. 10). These spherical droplet-shaped pores with a high degree of connectivity are usually formed by spinodal decomposition [8,31]. It is evident that a high degree of phase separation has occurred in this glass series. The porous morphology observed had a long range order, with a narrow pore size distribution. This is a trademark of spinodal decomposition. Pore size was also found to increase with increasing heat-treatment dwell time, consistent with mercury porosimetry findings (see Table 3). An interconnected structure consisting of two mutually penetrating interconnected phase was observed for all of the glasses, but the quality of the pore morphology varied across the series. The base glass AA showed excellent three dimensional pore definition. The pore size is uni-modal and on the order of 100 nm, which is in excellent agreement with the pore distribution observed in Fig. 8a. It is more difficult to explain the gas adsoption findings, i.e. pores on the order of 10 nm. It may well be that these are a result of gel trapped inside the pores, or equally, there may be micro- and meso-pores within the pore walls, which are beyond the resolution limit of the scanning electron microscope.

Glass CC and glass DD exhibited similar pore morphologies. Compared to glass AA, these glasses appeared to have a more open morphology, with narrow pore walls. Glass CC, in particular, showed a very high pore volume (see Table 3). Glass DD had a smaller mean pore diameter than glass CC, due to its higher zircon content. Glass EE again shows a highly interconnected pore structure. The sample heated for 14 h does not appear to have the same three-dimensional aspect as base glass AA. As the glass is heated-treated for longer times it shows signs of crystallising; the pores become less obvious, they appear to grow into one other. This effect would likely be exacerbated for longer hold times, so it may be difficult to generate a material with larger pores, if desired. For glass E-II, the formation of crystals is observed, especially when the heat-treatment dwell time was increased from 24 h to 63 h, leading to the loss of the porous structure.

Table 5 summarises the EDXS elemental analysis of porous glasses after heat-treatment and leaching. Unfortunately EDXS cannot detect boron but inferences can be made based on the presence of Zr. Bond valence models by Connelly et al. [32] showed that BO_3 bonds are more likely to form Zr–O–B than that of four-coordinated BO_4. For glasses CC and DD studied here, it is postulated that Zr formed Zr–O–^{III}B with BO_3, which was then completely eluted during leaching. No trace of Zr was detected by EDXS. An exception was observed for glasses EE and E-II, where a high presence of Zr was detected. An explanation lies in the ZrO_2 or $ZrSiO_4$ content (15 wt%) of the EE-series glasses. These authors believe that for $ZrO_2/ZrSiO_4$ contents > 11 wt% there are insufficient BO_3 groups available to form bonds with Zr. As a result, Zr moves to the silica-rich phase by forming Si–O–Zr bonds and thus remains in the porous glass skeleton after leaching.

3.4. Alkali resistance

The alkali resistance remains almost constant for glass AA–DD. As shown in Table 5, no Zr was detected in these glasses. It is therefore presumed that Zr migrated to the sodium-borate rich phase and was eluted during leaching. Therefore, it is not surprising that samples AA–DD showed similar alkali resistance. The small difference identified was due to their textural properties, i.e. surface area. The presence of Zr in glass EE gave rise to a significant improvement in alkali resistance as shown in Table 6. The alkali resistance of glass EE is 3–4 times superior to that of glass AA, which contains no ZrO_2 or $ZrSiO_4$. Porous glass (EE)

containing $ZrSiO_4$ was found to be more alkali resistant than that of glass (E-II), containing ZrO_2.

4. Conclusions

Thermal analysis was used to determine glass transition temperatures and crystallisation temperatures of the sodium borosilicate glass system which contained additions of ZrO_2 and $ZrSiO_4$. Increasing the $ZrSiO_4$ content increased the glass transition temperature. The glasses studied here were heat-treated at 650 °C for durations of 14, 24 and 63 h, causing the glasses to phase separate by spinodal decomposition. Leaching was used to remove the sodium-borate rich phase and leave behind a skeletal structure consisting mainly of silica and zirconia. This porous structure had finely distributed macro-pores, with the main concentrations around 100 nm. Additions of $ZrSiO_4$ to the glass system hindered the growth rate of phase separation. As a result, the mean pore size of the porous glass decreased. A linear relationship was observed between mean pore size and the square root of heat-treatment dwell time. For longer heat-treatment times, the mean pore size increased. Scanning electron microscopy showed that the glass series AA–EE formed interconnected porosity. No trace of Zr was detected by EDXS for glasses with $ZrSiO_4$ content < 15 wt%. Zr was only detected in porous glass skeletons for $ZrSiO_4$ contents > 15 wt%. The porous glasses containing Zr were more alkali resistant than the basic sodium borosilicate glass.

References

[1] W. Haller, Application of controlled pore glass in solid phase biochemistry, in: W.H. Scouten (Ed.), Solid Phase Biochemistry, John Wiley & Sons, New York, 1983, pp. 535–597.

[2] J.E. Shelby, M. Lopes, Introduction to Glass Science and Technology, second ed., The Royal Society of Chemistry, Cambridge, 2005.

[3] W. Du, K. Kuraoka, T. Akai, T. Yazawa, Study of kinetics of the phase separation in sodium borate glasses, Journal of Materials Science 35 (2000) 3913–3921.

[4] M.J. Plodinec, Borosilicate glasses for nuclear waste imobilisation, Glass Technology 41 (2000) 186–192.

[5] J.D. Vienna, Nuclear waste vitrification in the United States: recent developments and future options, International Journal of Applied Glass Science 1 (2010) 309–321.

[6] J. Park, S. Lee, Mechanism of preventing crystallization in low-firing glass/ceramic composite substrates, Journal of the American Ceramic Society 78 (1995) 1128–1130.

[7] R.R. Tummala, Ceramic and glass-ceramic packaging in the 1990s, Journal of the American Ceramic Society 74 (1991) 895–908.

[8] K. Nakashima, K. Noda, K. Mori, Time–temperature–transformation diagrams for borosilicate glasses and preparation of chemically durable porous glasses, Journal of the American Ceramic Society 80 (1997) 1101–1110.

[9] S. Scholes, F.C.F. Wilkinson, Glassy phase separation in sodium borosilicate glasses, Discussions of the Faraday Society 50 (1970) 175–181.

[10] N. Ford, R. Todhunter, Applications of microporous glasses, in: M.H. Lewis (Ed.), Glasses and Glass-Ceramics, Chapman and Hall, New York, 1989, pp. 203–225.

[11] A. Jungbauer, Chromatographic media for bioseparation, Journal of Chromatography A 1065 (2005) 3–12.

[12] R.W. Stout. 1986, Metal Oxide Stabilized Chromatography Packings, US Patent, no. 4,600,646.

[13] Y. Murakami. 1987, Method of Strengthening the Alkali Resistance of a Porous Glass, US Patent, no. 4,661,138.

[14] K. Eguchi, H. Tanaka, T. Yamaguro, T. Yazawa. 1988. Chemically Durable Porous Glass and Process for the Manufacture Thereof, US Patent, no. 4,778,777.

[15] K. Wada, Y. Tsurita. 1990. Porous Glass and Process for its Production, US Patent, no. 4,978,641.

[16] C.V. McNeff, P.W. Carr, S.J. Rupp, D.R. Stoll, D.R. Hawker, L.D. Zigan, K.G. Johnson. 2005. High Stability Porous Metal Oxide Spherules Used for One-Step Antibody Purifications, US Patent, no. 6,846,410.

[17] M. Hasanuzzaman, M. Sajjia, A. Rafferty, A.G. Olabi, Thermal behaviour of zircon/zirconia-added chemically durable borosilicate porous glass, Thermochimica Acta 555 (2013) 81–88.

[18] M.S. Hernández-Crespo, M. Romero, J.M. Rincón, Nucleation and crystal growth of glasses produced by a generic plasma arc-process, Journal of the European Ceramic Society 26 (2006) 1679–1685.

[19] J.W. Dodd, K.H. Tonge, Thermal Methods (Analytical Chemistry by Open Learning), John Wiley & Sons, London, 1987.

[20] J. Kerc, S. Srcic, Thermal analysis of glassy pharmaceuticals, Thermochimica Acta 248 (1995) 81–95.

[21] M. Kukizaki, Large-scale production of alkali-resistant Shirasu porous glass (SPG) membranes: Influence of ZrO_2 addition on crystallization and phase separation in Na_2O–CaO–Al_2O_3–B_2O_3–SiO_2 glasses; and alkali durability and pore morphology of the membranes, Journal of Membrane Science 360 (2010) 426–435.

[22] T. Wakasugi, L.L. Burgner, M.C. Weinberg, A DTA study of crystal nucleation in Na_2O–SiO_2 glasses, Journal of Non-Crystalline Solids 244 (1999) 63–73.

[23] A. Hu, K. Liang, M. Li, D. Mao, Effect of nucleation temperatures and time on crystallization behavior and properties of Li_2O–Al_2O_3–SiO_2 glasses, Materials Chemistry and Physics 98 (2006) 430–433.

[24] A.P. Novaes, Oliveira de, A. Bonamartini Corradi, L. Barbieri, C. Leonelli, T. Manfredini, The effect of the addition of $ZrSiO_4$ on the crystallisation of $30Li_2O/70SiO_2$ powdered glass, Thermochimica Acta 286 (1996) 375–386.

[25] H.E. Kissinger, Variation of peak temperature with heating rater in differential thermal analysis, Journal of Research of the National Bureau of Standards 57 (1956) 217–221.

[26] M.M. Lima, R. Monteiro, Characterisation and thermal behaviour of a borosilicate glass, Thermochimica Acta 373 (2001) 69–74.

[27] M.J. Cattell, T.C. Chadwick, J.C. Knowles, R.L. Clarke, D.Y. D. Samarawickrama, The nucleation and crystallization of fine grained leucite glass-ceramics for dental applications, Dental Materials 22 (2006) 925–933.

[28] D. Enke, F. Janowski, W. Gille, W. Schwieger, Structure and texture analysis of colloidal silica in porous glasses, Colloids and Surfaces A: Physicochemical and Engineering Aspects 187–188 (2001) 131–139.

[29] J. Rouquerol, G.V. Baron, R. Denoyel, H. Giesche, J. Groen, P. Klobes, et al., The characterization of macroporous solids: An overview of the methodology, Microporous and Mesoporous Materials 154 (2012) 2–6.

[30] Quantacrome Instruments Nova Series e specification, High-Speed Surface Area and Pore Size Analyzer System, Quantacrome Instruments, 2008.

[31] B.R. Wheaton, A.G. Clare, Evaluation of phase separation in glasses with the use of atomic force microscopy, Journal of Non-Crystalline Solids 353 (2007) 4767–4778.

[32] A.J. Connelly, N.C. Hyatt, K.P. Travis, R.J. Hand, E.R. Maddrell, R.J. Short, The structural role of Zr within alkali borosilicate glasses for nuclear waste immobilization, Journal of Non-Crystalline Solids 357 (2011) 1647–1656.